Original Article

MOLECULAR METABOLISM

BMI-anchored transcriptomics uncovers oxidative and inflammatory poles of obesity heterogeneity

Su Yin-Yuan[1,2,12,1], Bundalian Linnaeus[2,3,1], Chen Yin-Cheng[1,2], Gjermeni Erind[4], Gille Benedikt[5], Richter Sandy[6], Jasaszwili Mariami[6], Palma-Vera Sergio Eliseo[5], Hoffmann Anne[7], Ghosh Adhideb[8], Wolfrum Christian[8], Blüher Matthias[7,9,10], Peleg Shahaf[5], Garten Antje[6,11], Le Duc Diana[2,3,*], Lin Chen-Ching[1,2,]**

ABSTRACT

Background: BMI remains the dominant clinical index of obesity, but does not resolve adipose molecular programs that distinguish metabolic resilience from vulnerability.

Methods: Among 1,479 available human visceral adipose RNA-seq profiles, 1,298 samples from individuals with BMI 30—60 were included in the primary modeling cohort. Using BMI as a phenotypic anchor, we fit a LASSO regression model to derive transcriptome-predicted BMI and applied the resulting BMI-anchored transcriptomic model to mouse selection lines with divergent obesity phenotypes. In humans, directional discordance between measured and predicted BMI was used to define transcriptome-derived metabolically healthy obesity-like (MHO-like) and metabolically unhealthy obesity-like (MUO-like) states and to characterize pathophysiologic variation beyond measured BMI.

Results: Model-selected genes converged on immune, metabolic, mitochondrial, growth, structural-remodeling, and proteostasis programs. Cross-species application showed that BMI-anchored transcriptomic scores more closely tracked adipose-tissue content than body-size condition factor, distinguishing lipid-anabolic and inflammatory features of obesity-prone DU6 mice from the oxidative-catabolic phenotype of DU6P mice characterized by increased muscle mass. Gene-level associations with the transcriptomic score mirrored DU6-associated expression changes, linking the cross-species axis to an obesity-vulnerable adipose state. In humans, MHO-like individuals showed enhanced mitochondrial energy-production programs and more favorable glycemic and lipid profiles, whereas MUO-like individuals showed stress-adaptive metabolic remodeling and greater cardiometabolic medication use. In a separate, non-overlapping validation cohort, projection onto the primary-cohort PCA space retained a signal associated with insulin resistance that remained essentially unchanged after adjustment for sex.

Conclusions: These findings support a conserved adipose transcriptomic axis linking oxidative metabolic resilience to healthier obesity and lipid-inflammatory remodeling to metabolic vulnerability.

© 2026 The Authors. Published by Elsevier GmbH. This is an open access article under the CC BY-NC license (http://creativecommons.org/licenses/by-nc/4.0/).

Keywords Obesity; Adipose transcriptomics; Cross-species model; Adipose tissue metabolism; BMI-Anchored transcriptomic model; Visceral adipose tissue

1. INTRODUCTION

Obesity and its closely related cardiometabolic comorbidities, e.g. cardiovascular disease, type 2 diabetes mellitus (T2D), hypertension, and metabolic dysfunction-associated steatotic liver disease, rank among the leading causes of morbidity and mortality worldwide [1]. Beyond these disorders, obesity substantially contributes to other major causes of death [2], including cancer [3], neurodegenerative

[1]Institute of Biomedical Informatics, National Yang Ming Chiao Tung University, Taipei, Taiwan [2]Institute for Clinical Genetics, University Hospital Carl Gustav Carus at TUD Dresden University of Technology and Faculty of Medicine of TUD Dresden University of Technology, Dresden, Germany [3]Institute for Human Genetics, Leipzig University Medical Center, Leipzig, Germany [4]Department of Cardiac Rehabilitation, Falkenstein Clinic, Bad Schandau, Germany [5]Research Institute for Farm Animal Biology (FBN), Dummerstorf, Germany [6]Center for Pediatric Research, Hospital for Children and Adolescents, Leipzig University, Leipzig, Germany [7]Helmholtz Institute for Metabolic, Obesity and Vascular Research (HI-MAG), Helmholtz Center Munich at the Leipzig University and University of Leipzig Medical Center, Leipzig, Germany [8]Laboratory of Translational Nutrition Biology, Institute of Food, Nutrition and Health, ETH Zürich, Schwerzenbach, Switzerland [9]Leipzig University Medical Center, Divisions of Endocrinology and Nephrology, University of Leipzig, Leipzig, Germany [10]LeiCeM - Leipzig Center of Metabolism, Leipzig University, Leipzig, Germany [11]German Center for Child and Adolescent Health (DZKJ), partner site Leipzig-Dresden, Germany [12]Center for Computational and Systems Biology, National Taiwan University, Taipei, Taiwan

[1] These authors contributed equally.

*Corresponding author. E-mail: chenching.lin@nycu.edu.tw (L.D. Diana).

**Corresponding author. E-mail: diana.leduc@ukdd.de (L. Chen-Ching).

Received June 11, 2026 • Revision received October 9, 2026 • Accepted October 15, 2026 • Available online 23 October 2026

https://doi.org/10.1016/j.molmet.2026.102462

 © 2026 The Authors. Published by Elsevier GmbH. This is an open access article under the CC BY-NC license (http://creativecommons.org/licenses/by-nc/4.0/).

diseases [4], and chronic kidney disease [5]. However, obesity is not a biologically uniform condition. Individuals with excess adiposity can differ substantially in metabolic status, disease susceptibility, and clinical course [6,7].

Overweight and obesity are defined as abnormal or excessive body fat accumulation that poses a health risk; a body mass index (BMI) $\geq$25 kg/m^2 is considered overweight and $\geq$30 kg/m^2 is classified as obesity [8]. However, BMI can both under- and overestimate adiposity and provides inadequate information about individual health risk [9,10]. Individuals with similar BMI, or even similar body-fat percentage, can exhibit markedly different cardiometabolic profiles [11,12]. The "personal fat threshold" hypothesis posits that the cardiometabolic impact of weight depends on each person's capacity for safe fat storage, thereby explaining obesity-related heterogeneity, such as in T2D [13,14]. Nonetheless, BMI remains the dominant framework for defining obesity in both clinical and research settings [9,10], underscoring the need for molecular approaches that better capture the underlying biology of adipose tissue and its contribution to metabolic health.

Murine models have been pivotal for discoveries in metabolism and aging, yet identifying systems that recapitulate human metabolic heterogeneity remains challenging. This challenge is compounded by the limited availability of cross-species transcriptional frameworks that directly connect human obesity heterogeneity with experimentally tractable animal biology [15,16]. The non-inbred DU6 mouse is a particularly informative model of obesity [17]. DU6 was derived from a polygenic founder population (FZTDU) established in 1969/1970 by crossing four outbred strains with four inbred strains; selection for high body mass at six weeks began in 1975 with 60–80 mating pairs per generation, while an unselected control line was maintained throughout [18]. Adult DU6 mice average ~110 g—substantially heavier than control FZTDU mice (~44 g)—and accumulate ~4% intra-abdominal fat versus ~1% in controls. DU6 mice exhibit multiple cardiometabolic abnormalities characteristic of metabolically unhealthy obesity (MUO) [19]. In contrast, the related mouse line DU6P, selected for high protein mass at six weeks, shows a "giant yet lean" phenotype with high muscle content [18,20]. These opposing phenotypes provide a tractable system to disentangle adipose tissue-driven lipid accumulation from lean-mass accrual.

To investigate whether obesity-related molecular states are conserved across species, we developed a BMI-anchored transcriptomic model using visceral adipose tissue gene-expression profiles from 1,298 human patients, using BMI as a practical training anchor (Fig. 1A). We focused on visceral adipose tissue (VAT) because this depot is closely linked to cardiometabolic disease, systemic metabolic regulation, and adipose inflammation, making it particularly well suited for interrogating molecular heterogeneity in obesity [21–23]. We then extended it across species by mapping high-confidence orthologous genes to adipose tissue samples from three well-characterized mouse lines: DU6 (obese-prone), DU6P (lean/protein-prone), and FZTDU (unselected control). This framework leverages adipose tissue transcriptomes to test whether conserved molecular programs differentiate metabolically unhealthy from healthier obesity states and to probe mechanisms underlying lipid accumulation versus oxidative efficiency.

2. RESULTS

Construction, stability, and functional annotation of the BMI-anchored transcriptomic model.

To investigate molecular mechanisms underlying obesity progression, we established a BMI-anchored transcriptomic model from visceral adipose tissue RNA-sequencing profiles. RNA-sequencing data from 1,298 human visceral adipose tissue samples from individuals with 30 $\leq$ BMI $<$60 kg/m^3 were used as input features (Fig. S1), with measured BMI serving as the response variable. BMI was selected because it is routinely collected and clinically relevant, whereas other metabolic parameters contained substantial missing data and were therefore less suitable as a common phenotypic anchor. Rather than developing a clinically deployable BMI prediction model, we used BMI as a practical and widely available quantitative anchor to derive a transcriptomic representation of obesity-related variation. The LASSO regularization parameter was selected to preserve BMI-related rank structure, targeting a Spearman's ρ of approximately 0.8 between the predicted and measured BMI. At the selected regularization parameter ($\alpha = 0.123$), 458 of the 16,042 candidate orthologous genes retained non-zero coefficients. The resulting predicted BMI served as a BMI-anchored transcriptomic representation for subsequent analyses (Fig. 1A).

We next evaluated the robustness of gene selection to perturbation of the modeling cohort by repeatedly refitting the model using 40–90% of the 1,298 participants. With α fixed at 0.123, genes belonging to the primary 458-gene set were consistently reselected more frequently than the remaining candidate genes across all sampling fractions (Fig. 1B and Supplementary Methods). The mean reselection probability of primary-model genes increased from 20.1% at 40% subsampling to 65.6% at 90% subsampling, whereas the corresponding mean for non-primary genes remained low, ranging from approximately 1.0%–1.6%. Because use of a fixed α can change model sparsity as sample size varies (Fig. S2), we repeated the analysis while adjusting α to approximately match the number of selected genes in the primary model. Under this matched-sparsity condition, the same pattern was retained: mean reselection probability of primary-model genes increased from 22.6% at 40% subsampling to 65.6% at 90%, whereas non-primary genes remained infrequently selected, with mean probabilities of approximately 1.0–2.3% (Fig. 1C and Supplementary Methods). Thus, preferential reselection of primary-model genes was observed under both fixed-α and sparsity-controlled subsampling.

We next examined whether the observed gene-selection pattern depended on the specific regularization setting used for the primary model (Supplementary Methods). Across 81 α values yielding training Spearman's ρ values between 0.7 and 0.9, the number of selected genes ranged from approximately 311 to 658. Across the full set of 81 models, 703 unique genes were selected at least once. Primary-model genes were strongly concentrated among the most consistently selected features: 281 of the 458 primary genes retained non-zero coefficients at every examined α value, whereas none of the 245 non-primary genes selected under at least one alternative setting were selected across the complete regularization range (two-sided Fisher's exact p-value $= 2.25 \times 10^{-73}$; Fig. 1D). Together, these analyses indicate that the primary model captures a preferentially selected transcriptomic feature set that is robust to both perturbation of cohort composition and variation in regularization.

To assess the biological interpretability of the model-selected genes, we performed gene set enrichment analysis (GSEA) to examine whether these data-driven features converged on coherent biological programs, including pathways related to obesity and metabolism. Enriched Gene Ontology (GO) terms were subsequently grouped into functional themes (Supplementary Methods), and their normalized

 © 2026 The Authors. Published by Elsevier GmbH. This is an open access article under the CC BY-NC license (http://creativecommons.org/licenses/by-nc/4.0/).

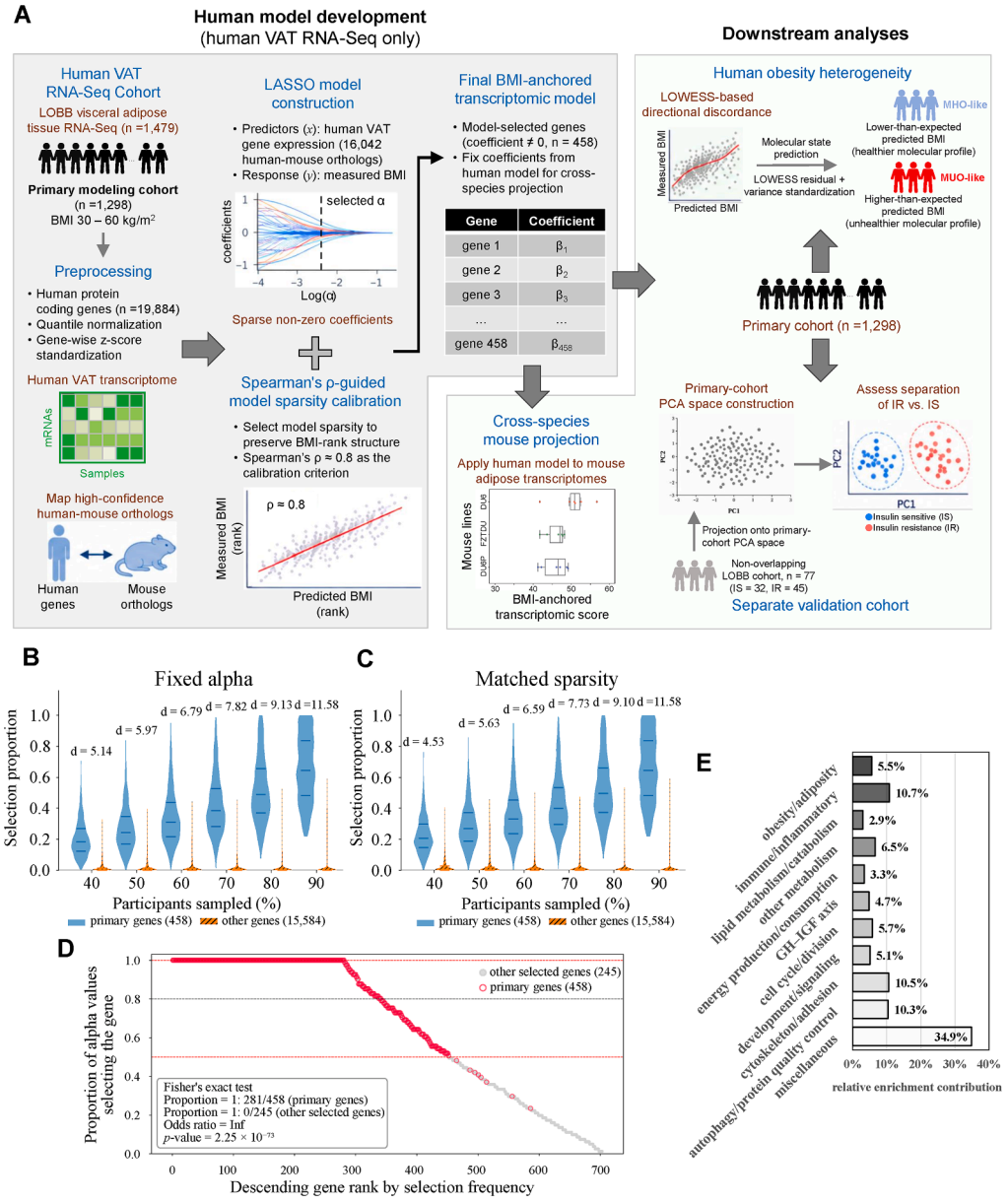


Figure 1: Construction, stability, and functional characterization of the BMI-anchored transcriptomic model. (A) Schematic overview of the study workflow. A BMI-anchored transcriptomic model was developed from human VAT RNA-seq data and subsequently applied to perform cross-species projection in mouse adipose transcriptomes, characterize human obesity heterogeneity, and evaluate a separate insulin-sensitivity cohort. (B) Gene-level selection-frequency distributions using fixed α. For each gene, selection frequency was defined as the proportion of 500 iterations in which its LASSO coefficient was non-zero. Distributions are shown separately for the 458 primary model-selected genes and the remaining 15,584 candidate genes. Internal lines indicate the 25th, 50th, and 75th percentiles, and d denotes Cohen's d for the difference between the two distributions. Differences in selection-frequency distributions were assessed using two-sided Mann–Whitney U tests, with *p*-values adjusted across the six sampling fractions using the Holm method. Primary model-selected genes showed markedly higher selection frequencies at every sampling fraction (all Holm-adjusted *p*-values $<1.1 \times 10^{-296}$). (C) Corresponding gene-level selection-frequency distributions after approximately matching model sparsity to the 458-gene primary model. Statistical comparisons were performed as in b, and primary model-selected genes again showed substantially higher selection frequencies than other candidate genes across all sampling fractions (all Holm-adjusted *p*-values $<7.4 \times 10^{-277}$). (D) Gene-selection stability was evaluated across 81 LASSO regularization parameters yielding training Spearman's ρ values between 0.7 and 0.9. For each gene selected under at least one of these settings, selection frequency was defined as the proportion of α values at which the gene retained a non-zero coefficient, and genes were ranked accordingly. Genes selected in the primary model ($\alpha = 0.123$; 458 genes, corresponding to Spearman's $\rho \approx 0.8$) are outlined in red, whereas all other selected genes are shown in gray. Of the 458 primary-model genes, 281 were selected at every examined α value, compared with none of the 245 non-primary genes (two-sided Fisher's exact test, *p*-value $= 2.25 \times 10^{-73}$; OR $\rightarrow \infty$ because no non-primary gene had a selection frequency of 1). (E) Functional enrichment of genes selected by the BMI-anchored transcriptomic model. Enriched Gene Ontology biological processes were grouped into higher-order functional categories. The relative enrichment contribution of each category was calculated as the sum of NES values for all GO terms assigned to that category divided by the summed NES values across all terms, expressed as a percentage.

 © 2026 The Authors. Published by Elsevier GmbH. This is an open access article under the CC BY-NC license (http://creativecommons.org/licenses/by-nc/4.0/).

enrichment scores (NES) were used to quantify the relative contribution of these functional categories (Fig. 1E and Fig. S3).

The functional annotation identified contributions from obesity/adiposity (5.5%) and immune/inflammatory (10.7%) processes, including cytokine regulation, adipose tissue inflammation, and glucose-responsive pathways, highlighting the close interplay between immune signaling and adipose metabolic regulation. Metabolic programs included lipid metabolism/catabolism (2.9%) and other metabolic processes (6.5%), encompassing lipid-handling, polyamine, and nucleotide-associated pathways. Additional functional themes involved energy production/consumption (3.3%), the GH—IGF axis (4.7%), cell cycle/division (5.7%), development/signaling (5.1%), and cytoskeleton/adhesion (10.5%), collectively representing cellular energetics, hormone signaling, proliferation, and structural remodeling. Autophagy/protein quality control accounted for a further 10.3% of the functional enrichment contribution.

Overall, the BMI-anchored model identified transcriptomic features that retained preferential selection across complementary stability analyses and converged on coherent biological programs spanning immune regulation, metabolism, mitochondrial energetics, growth, proteostasis, and structural remodeling. These findings support the use of the selected transcriptomic features as a biologically organized representation of BMI-associated adipose variation for the subsequent cross-species and human heterogeneity analyses.

2.1. Application of the model to mouse lines with divergent obesity phenotypes

To assess the cross-species relevance of our model, we applied it to transcriptomic data of epigonadal adipose tissue from three well-characterized mouse selection lines: DU6, selected for high body weight; DU6P, selected for high protein mass; and FZTDU, the unselected control. The condition factor (CF), calculated as body weight (g)/body length $(cm)^3$, ranked DU6 $\approx$ DU6P $>$ FZTDU (Fig. 2A). In contrast, the group mean values of relative white adipose tissue content followed the order DU6 $>$ DU6P $\approx$ FZTDU (Fig. 2A), revealing a discrepancy between gross phenotype (CF) and adipose tissue composition. Consistent with this divergence, independent histological analyses performed in a separate cohort showed adipose morphological differences among the mouse lines, including adipocyte hypertrophy and inflammatory remodeling in DU6 (Supplementary Information and Fig. S4).

When the BMI-anchored transcriptomic model was applied to mouse adipose transcriptomes, the resulting BMI-anchored transcriptomic scores ranked DU6 $>$ DU6P $\approx$ FZTDU (Fig. 2B), matching the order of epigonadal white adipose content more closely than the order of CF. This indicates that the BMI-anchored transcriptomic score is more strongly aligned with adipose tissue content than with body-size measures in these mouse lines. Sensitivity analyses using alternative BMI ranges for human model construction showed that the characteristic elevation of the DU6 score was preserved when participants with BMI <30 kg/m^3 were included and when the upper BMI restriction was removed (Fig. S5). Thus, the BMI-anchored transcriptomic score shows a pattern more closely aligned with adipose tissue composition than with condition factor across the three mouse lines.

2.2. Opposing lipid-anabolic and oxidative-catabolic states define DU6 and DU6P along the BMI-anchored transcriptomic axis

To determine whether the BMI-anchored transcriptomic model captures biologically meaningful distinctions in obesity states, we first performed Gene Set Enrichment Analysis (GSEA) to assess broad functional trends between DU6 (obese-prone) and DU6P (lean/protein-prone) mice.

Enrichment profiles revealed contrasting transcriptional programs between the two lines (Fig. 3A and Figs. S6 and S7). Relative to DU6P, DU6 showed stronger enrichment of immune/inflammatory pathways, including cytokine regulation, leukocyte migration, and mast cell degranulation, alongside broad activation of cell cycle/division processes, consistent with comparatively greater inflammatory activation and proliferative remodeling. By contrast, DU6P showed relative enrichment of growth and tissue regulation, dominated by energy production/consumption and development/signaling processes. Additional enrichment of lipid metabolism/catabolism and other metabolism in DU6P suggested metabolic flexibility, whereas immune/inflammatory and cell cycle/division were notably absent. Together, these findings indicate a functional divergence between the two lines, with DU6 biased toward immune and proliferative programs and DU6P biased toward energetics- and development-associated programs.

Because GSEA captures distributed transcriptome-wide signals, we next performed up-regulated differentially expressed gene (DEG) enrichment analysis to obtain sharper resolution of functional modules (Fig. 3B, Table S1, and Supplementary Methods). Genes identified by DESeq2 with an adjusted p-value <0.05 and log2 fold change >0 were defined as up-regulated DEGs. This analysis revealed opposing metabolic programs between the two lines. In DU6, lipid synthesis and storage pathways were strongly enriched (OR $\approx$ 76.5, p-value $= 3.8 \times 10^{-11}$), consistent with an anabolic program favoring lipid accumulation. In DU6P, enrichment was dominated by oxidative metabolism, including multiple respiratory chain complexes: Complex I (OR $\approx$ 28.4, p-value $= 3.75 \times 10^{-12}$), Complex II (OR $\approx$ 27.1, p-value $= 0.05$), Complex III (OR $\approx$ 69.0, p-value $= 1.13 \times 10^{-7}$), Complex IV structural components (OR $\approx$ 31.8, p-value $= 2.0 \times 10^{-6}$) and assembly factors (OR $\approx$ 10.9, p-value $= 0.02$), and Complex V/ATP synthase (OR $\approx$ 27.7, p-value $= 3.5 \times 10^{-7}$). DU6P was also enriched in mitochondrial ribosomal proteins (OR $\approx$ 5.57, p-value $= 2.8 \times 10^{-3}$), mitochondrial translational activators (OR $\approx$ 30.7, p-value $= 2.8 \times 10^{-4}$), and mitochondrial regulatory machinery (OR $\approx$ 15.3, p-value $= 2.1 \times 10^{-7}$), defining a strong OXPHOS-centered program. Furthermore, DU6P exhibited expanded fatty acid oxidation (FAO) capacity, encompassing mitochondrial FAO enzymes, ETF coupling factors, and peroxisomal biogenesis (OR $\approx$ 20.3, p-value $= 2.9 \times 10^{-8}$), underscoring a broad oxidative orientation. Analysis of the growth hormone (GH) signaling axis provided an additional discriminant feature. While the strict GH core set showed no significant difference between lines, the extended GH axis—incorporating downstream metabolic effectors—was significantly enriched in DU6P (OR $\approx$ 13.7, p-value $= 3.5 \times 10^{-4}$) but not in DU6 (OR $\approx$ 11.2, p-value $= 0.09$). This suggests that GH-axis-associated transcriptional regulation is more strongly represented in DU6P and may be linked to its enhanced oxidative program.

To test whether these opposing transcriptional states were also aligned with the BMI-anchored transcriptomic axis at the gene level, we compared differential-expression effect sizes with gene-wise correlations with BMI-anchored transcriptomic score across all three pairwise mouse-line contrasts (Fig. 3C). Strong positive concordance was observed for differential gene expression patterns involving DU6: log2 fold changes were positively associated with Spearman correlation coefficients in both DU6 vs DU6P (Pearson $r = 0.406$; Spearman's $\rho = 0.552$) and DU6 vs FZTDU (Pearson $r = 0.385$; Spearman's $\rho = 0.602$). In contrast, DU6P vs FZTDU showed only minimal association (Pearson $r = 0.066$; Spearman's

 © 2026 The Authors. Published by Elsevier GmbH. This is an open access article under the CC BY-NC license (http://creativecommons.org/licenses/by-nc/4.0/).

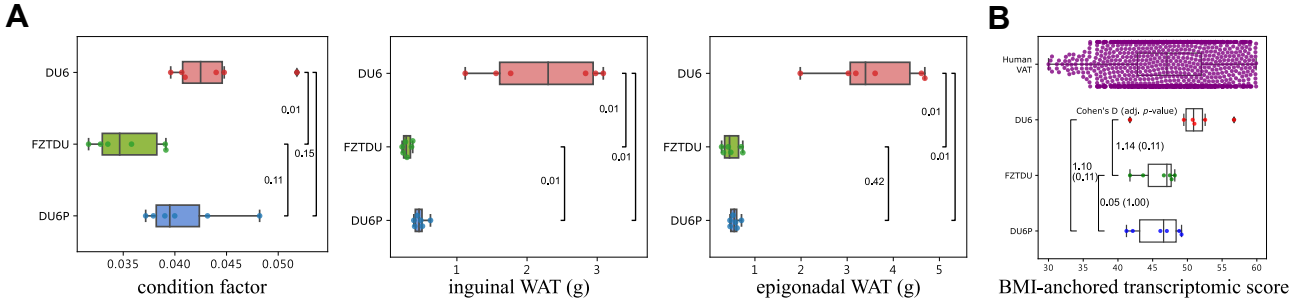


Figure 2: Phenotypic and molecular divergence among DU mouse lines. (A) Boxplots showing the distribution of the condition factor (g/cm^3) and normalized white adipose tissue (WAT) weights, calculated as depot weight divided by total body weight, from the inguinal and epigonadal depots across the mouse lines DU6, FZTDU, and DU6P. Mouse lines are ordered as follows: DU6 (obesity-prone), FZTDU (control), and DU6P (bred for increased protein mass). Pairwise comparisons were performed using two-sided Wilcoxon rank-sum tests. *P*-values were adjusted separately within each phenotype for the three pairwise comparisons using the Holm—Bonferroni method; adjusted *p*-values are shown in the figure. (B) Cross-species projection of the BMI-anchored transcriptomic model. Each point represents an individual human VAT sample (BMI 30—60, $n = 1{,}298$) and adipose tissue from the mouse lines DU6, FZTDU, and DU6P, and the x-axis indicates the BMI-anchored transcriptomic score. Boxplots summarize group distributions, and effect sizes (Cohen's *d*) are shown for pairwise comparisons. Pairwise comparisons were performed using two-sided Wilcoxon rank-sum tests, with *p*-values adjusted for the three pairwise comparisons using the Holm—Bonferroni method. Adjusted *p*-values are shown in the figure. The BMI-anchored transcriptomic score ranking (DU6 > FZTDU ≈ DU6P) mirrors adipose-tissue accumulation rather than body size, while aligning with the human visceral reference distribution.

$\rho = 0.087$). This pattern indicates that the BMI-anchored transcriptomic axis does not simply reflect generic inter-line divergence, but preferentially tracks the molecular program associated with the DU6 state. Thus, the mouse analysis provides cross-species support that the BMI-anchored transcriptomic model captures a conserved adiposity-related state. In this framework, DU6 corresponds to the obesity-vulnerable, lipid-anabolic pole of the model, whereas DU6P corresponds to an oxidative-catabolic and metabolically resilient counter-state.

Taken together, these analyses identify DU6 and DU6P as two opposing adipose tissue transcriptional configurations: one biased toward lipid accumulation, inflammatory remodeling, and obesity vulnerability, and the other toward mitochondrial function, substrate oxidation, and metabolic resilience. The strong alignment of the BMI-anchored transcriptomic axis with differential gene expression patterns involving DU6 further supports the conclusion that this cross-species transcriptomic model captures a biologically meaningful obesity-related state rather than reflecting nonspecific inter-line differences, and suggests that the model may be especially useful for interrogating pathogenic adiposity and molecular remodeling associated with obesity progression.

2.3. Transcriptomic discordance between measured and predicted BMI stratifies MHO-like and MUO-like obesity states

To explore the utility of our BMI-anchored transcriptomic model in understanding obesity heterogeneity, we examined directional discordance between predicted and measured BMI across participants. According to the LOWESS-based framework described in the Methods (Fig. 4A), individuals whose measured BMI was higher than expected from their predicted BMI were classified as transcriptome-derived metabolically healthy obesity—like (MHO-like), whereas those whose measured BMI was lower than expected from their predicted BMI were classified as transcriptome-derived metabolically unhealthy obesity—like (MUO-like). These designations reflect transcriptome-derived resemblance to relatively metabolically favorable or unfavorable obesity states and do not represent conventional clinical diagnoses of MHO or MUO. This framework therefore identified participants whose gene expression-derived BMI predictions were discordant with their measured BMI. MHO-like participants had a measured BMI higher than expected from their predicted BMI, consistent with a relatively favorable molecular profile despite elevated BMI. In contrast, MUO-like participants had a measured BMI lower than expected from their predicted BMI, consistent with a comparatively adverse molecular profile.

Analysis of up-regulated genes in MHO-like patients revealed enrichment dominated by energy production/consumption (55%), suggesting strong signals in mitochondrial energetics, including oxidative phosphorylation and ATP synthesis—coupled electron transport (Fig. 4B and Fig. S8). Secondary contributions were categorized as other metabolism, including RNA biosynthesis, intracellular sodium ion homeostasis, and nucleic acid metabolism. Together, these results suggest that MHO-like patients maintain an enhanced capacity for mitochondrial energy production and metabolism, reflecting coordinated growth and metabolic efficiency.

In contrast, the MUO-like profile displayed a distinct enrichment pattern characterized by broad transcriptional remodeling (Fig. 4B and Fig. S9). The strongest enrichment was observed in other metabolism, which included RNA processing and oxoacid and nucleotide metabolism. Substantial signals were also detected in autophagy/protein quality control, reflecting activation of proteostatic and stress-adaptive mechanisms, and in lipid metabolism/catabolism, represented by pathways such as fatty acid β-oxidation. Collectively, these results indicate that genes up-regulated in MUO-like patients primarily participate in metabolic regulation, proteostasis, and lipid catabolism that support stress adaptation and tissue remodeling.

Moreover, clinical parameters were broadly consistent with these molecular distinctions (Fig. 4C). MHO-like individuals exhibited significantly lower fasting plasma glucose (FPG, *p*-value $= 2.7 \times 10^{-6}$) and triglycerides (*p*-value $= 5.0 \times 10^{-7}$), along with higher HDL-cholesterol (*p*-value $= 8.7 \times 10^{-5}$), indicating their more favorable glycemic control and lipid handling. In contrast, MUO-like participants showed higher glycated hemoglobin (HbA1c, *p*-value $= 4.5 \times 10^{-7}$). Cardiometabolic medication use was also more frequent in MUO-like group, including acetylsalicylic acid (ASS, OR $= 6.45$, *p*-value $= 0.001$), beta blockers (OR $= 2.94$, *p*-value $= 2.8 \times 10^{-3}$), and diuretics (OR $= 2.43$, *p*-value $= 0.002$). Together, these findings support the transcriptome-based stratification and further highlight the physiological and metabolic heterogeneity within obesity.

We further evaluated the model in a separate, non-overlapping LOBB validation cohort characterized for insulin resistance. To assess whether the transcriptomic structure represented by the model-

 © 2026 The Authors. Published by Elsevier GmbH. This is an open access article under the CC BY-NC license (http://creativecommons.org/licenses/by-nc/4.0/).

selected genes was preserved, we first performed principal component analysis using the model-selected genes in the primary cohort. The insulin-resistance–characterized samples were then projected onto this fixed PCA reference space using the loadings derived from the primary cohort. In this projected space, PC1 significantly distinguished insulin-resistant from insulin-sensitive individuals (Fig. 4D). Insulin-resistant individuals showed higher projected PC1 scores, with a moderate effect size (Cohen's $d = 0.54$) and statistical support from both Welch's t-test (p-value $= 0.02$) and the Mann–Whitney U test (p-value $= 0.03$). In parallel, the same LOWESS-based discordance framework was applied independently within the validation cohort, using quartile rather than decile standardization because of the smaller sample size. Lower quartile-standardized scores were directionally associated with higher odds of insulin resistance (OR $= 0.645$, 95% CI 0.359–1.156, p-value $= 0.14$), consistent with a more MUO-like state, although this association did not reach statistical significance. These analyses in the separate validation cohort suggest that the model-derived transcriptomic structure retains a modest but biologically relevant signal related to insulin resistance and metabolic vulnerability.

Together, these findings support a coherent model of obesity-related metabolic heterogeneity. In the primary human cohort, transcriptome-based stratification separated individuals with MHO-like obesity from those with MUO-like obesity, a distinction further supported by significant differences in clinical and biochemical parameters. Evaluation in the separate LOBB validation cohort further showed that the primary-cohort-derived PCA reference space preserved a detectable signal related to insulin resistance, while the discordance analysis performed within the validation cohort showed a directionally consistent relationship with insulin resistance status. Thus, unlike conventional obesity stratification based primarily on measured BMI, the transcriptome-based model captures a biologically meaningful

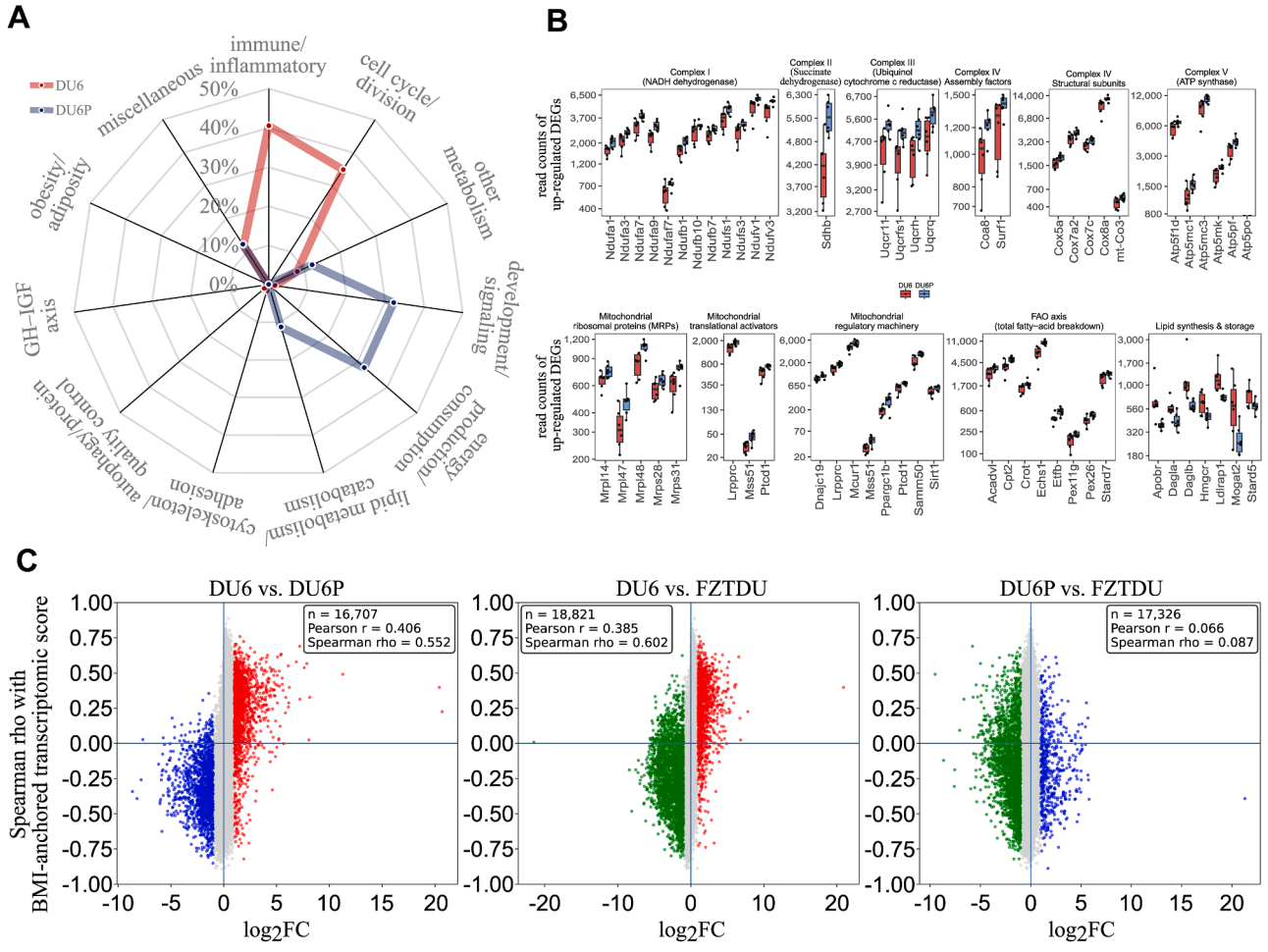


Figure 3: Comparative functional enrichment and mitochondrial pathway profiles in DU mouse lines. (A) Radar plot showing the relative enrichment contribution of functional categories between DU6 and DU6P lines. Categories include immune/inflammatory, cell cycle/division, other metabolism, development/signaling, energy production/consumption, lipid metabolism/catabolism, cytoskeleton/adhesion, autophagy/protein quality control, GH–IGF axis, obesity/adiposity, and miscellaneous. DU6 and DU6P exhibit distinct enrichment patterns, highlighting differential metabolic and signaling profiles. The relative enrichment contribution of each category was calculated from the proportional sum of NES values of functions within that category relative to the total NES. (B) Boxplots showing the read-count distributions of up-regulated differentially expressed genes (DEGs) assigned to representative mitochondrial and metabolic functional modules, including oxidative phosphorylation complexes (I–V), mitochondrial ribosomal proteins and translational activators, mitochondrial regulatory machinery, fatty-acid oxidation, and lipid synthesis and storage. Comparisons reveal a marked shift toward oxidative and catabolic pathways in DU6P, contrasting with the more anabolic and lipid-storage–oriented profile of DU6. (C) Scatter plots showing gene-level concordance between gene-expression correlation with the BMI-anchored transcriptomic score and differential expression across pairwise comparisons among DU6, DU6P, and FZTDU. The x axis indicates differential expression (log2 fold change, *log2FC*), and the y axis shows the corresponding Spearman correlation coefficient with the BMI-anchored transcriptomic score. Genes with $|\,log2FC\,| < 1$ are shown in light grey. Genes with $|log2FC| \geq 1$ are colored according to the mouse line in which they are up-regulated: DU6, red; DU6P, blue; and FZTDU, green. The vertical line indicates a *log2FC* of zero, and the horizontal line marks zero correlation.

 © 2026 The Authors. Published by Elsevier GmbH. This is an open access article under the CC BY-NC license (http://creativecommons.org/licenses/by-nc/4.0/).

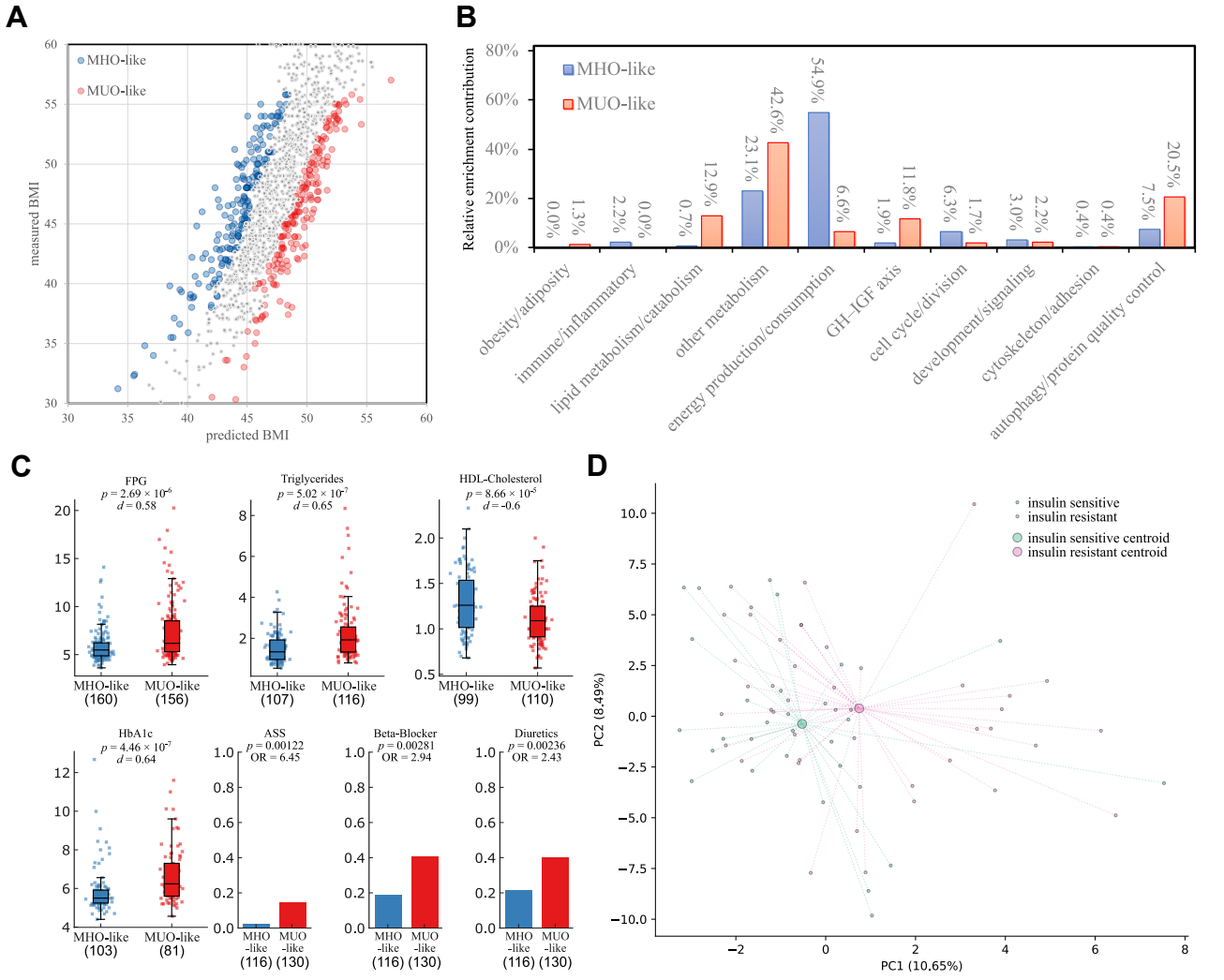


Figure 4: Molecular prediction of obesity subtypes and functional enrichment profiles. (A) Scatter plot comparing predicted versus measured BMI across individuals. Patients were stratified into MHO-like (blue) and MUO-like (red) groups based on a post-hoc LOWESS model, illustrating clear divergence between molecular and phenotypic obesity states. Grey points indicate intermediate individuals with decile-standardized discordance scores between −1 and 1. (B) Bar chart summarizing the relative enrichment contribution of functional categories for MHO-like and MUO-like subgroups. The MHO-like group is predominantly associated with energy production/consumption, whereas MUO-like shows higher contributions from other metabolism and autophagy/protein quality control pathways, highlighting distinct molecular mechanisms underlying obesity heterogeneity. Herein, the miscellaneous category was excluded and the remaining category contributions were renormalized to 100%; the complete distributions including miscellaneous terms are shown in Figs. S8 and S9. (C) For the clinical and biochemical comparison, three outliers were excluded: vis-2520, the MUO-like individual with the highest gGT; vis-2504, the MHO-like individual with the highest gGT; and vis-2149, the MUO-like individual with the highest triglyceride level. Seventy-seven clinical and biochemical parameters were screened, and variables passing the significance criteria are shown. Binary variables were analyzed using Fisher's exact test, and continuous variables were assessed using the Mann—Whitney U test. Effect sizes are reported as odds ratios (ORs) for binary variables, indicating the relative likelihood of a clinical feature in MUO-like compared with MHO-like, and as Cohen's d for continuous variables, calculated as MUO-like minus MHO-like; negative values therefore indicate higher levels in MHO-like. Nominal p-values and effect sizes are shown in each panel, whereas significance was determined using FDR-adjusted $q < 0.05$, with continuous variables additionally requiring |Cohen's d| > 0.4. Numbers in parentheses indicate the effective number of individuals available for each variable. (D) Projection of the separate, non-overlapping LOBB validation cohort onto the primary-cohort—derived PCA reference space. Individual samples classified as insulin sensitive or insulin resistant are projected onto the first two principal components, PC1 and PC2, which explain 10.65% and 8.49% of the variance, respectively. Larger points denote the subtype centroids, and dotted lines connect each individual to its assigned centroid, visualizing within-subtype dispersion and the separation between insulin-sensitive and insulin-resistant molecular states.

axis linking mitochondrial metabolic resilience to MHO-like states and insulin-resistance-associated vulnerability to MUO-like states.

3. DISCUSSION

In this study, we set out to determine whether conserved transcriptomic programs differentiate metabolically unhealthy from healthier obesity states. Our study establishes a transcriptome-based framework for dissecting the molecular underpinnings of obesity across human and mouse models. By integrating adipose tissue gene expression with machine learning, we demonstrated that transcriptomic features capture BMI-linked biological variation while preserving meaningful rank structure and revealing functional programs central to obesity biology. Our results are consistent with

 © 2026 The Authors. Published by Elsevier GmbH. This is an open access article under the CC BY-NC license (http://creativecommons.org/licenses/by-nc/4.0/).

human adipose tissue transcriptomic work showing that metabolic health is not completely BMI-dependent: bulk VAT profiling can stratify individuals with obesity into metabolically healthier versus unhealthier groups despite similar adiposity [24,25]. This separation may also reflect a continuum across stages of metabolic dysregulation [26]. In addition, compact transcriptomic signature models linking MUO to comorbidities (e.g., MASLD using liver/VAT expression) highlight the translational potential of expression-based risk subtyping [27]. Furthermore, functional enrichment analysis of genes selected by the BMI-anchored transcriptomic model identified programs spanning immune activation, lipid and energy metabolism, and cellular growth regulation, highlighting the multifactorial transcriptional features associated with BMI variation in adipose tissue. Importantly, cross-species validation confirmed that the model reflects adiposity-specific molecular signals rather than gross body size, since it could distinguish between DU6 and DU6P mouse lines that are similar in body weight to length ratio, but highly divergent in adipose tissue phenotype. Several other studies have used cross-species approaches to identify genes associated with obesity and fat deposition [28—30]. Liu et al. compared different machine learning methods to predict genes related to fat deposition in pigs, Acharjee et al. used publicly available human and mouse transcriptome data and machine learning to find obesity-associated genes that are common across species, and Wang et al. integrated the skeletal muscle transcriptome of obese pigs with publicly available transcriptional profiles and ATAC-seq human and mouse data.

A major strength of our approach lies in its ability to bridge anthropometric measurements with molecular signatures. Traditional metrics such as BMI or body weight provide only crude estimates of adiposity and fail to distinguish between metabolically healthy and unhealthy states. Our BMI-anchored transcriptomic model overcomes this limitation by identifying protective versus pathogenic molecular programs, including enhanced mitochondrial energetics in MHO-like individuals and remodeling/autophagy in MUO-like individuals. This capacity to extract biologically meaningful differences from transcriptomic data offers potential for improved stratification of obesity subtypes and for guiding precision interventions.

Nevertheless, certain limitations must be acknowledged. First, BMI was chosen as the quantitative modeling outcome due to its availability and clinical relevance, but it is an imperfect surrogate for adiposity and metabolic health [8,31,32]. Consistent with the internally calibrated nature of our modeling framework, evaluation in the separate LOBB validation cohort further highlighted this limitation: predicted BMI showed only weak and non-significant correlations with measured BMI in the separate cohort (Pearson $r = 0.15$; Spearman's $\rho = 0.12$). This indicates that the model does not transfer robustly as a direct quantitative regressor for absolute BMI across cohorts. However, weak agreement between predicted and measured BMI in the validation cohort does not necessarily imply that the learned transcriptomic signal is biologically uninformative. Rather, it suggests that BMI-anchored training may capture obesity-associated molecular variation that is not linearly reflected by measured BMI in a separate cohort. Importantly, projection of the separate cohort into the primary-cohort-derived PCA reference space preserved a detectable signal related to insulin resistance, supporting the biological relevance of the learned transcriptomic structure beyond direct BMI prediction.

To further determine whether the limited predictive performance primarily reflected the calibration-oriented design of the primary model, we performed an additional prediction-oriented analysis in which the regularization parameter was selected by inner 5-fold cross-validation to maximize out-of-sample BMI prediction. Even under this explicitly prediction-oriented framework, outer hold-out performance remained modest across training fractions, with median Spearman's ρ ranging from 0.148 to 0.212 (Fig. S10a). Notably, the resulting models were substantially sparser than the primary model, yet their selected genes were strongly enriched for genes contained in the primary 458-gene set. Thus, optimizing the modeling procedure specifically for BMI prediction did not substantially improve quantitative prediction, but continued to preferentially identify features represented in the primary transcriptomic model (Fig. S10b).

The subsampling analyses further clarify the nature of this feature-selection robustness. Across repeated 40—90% subsamples, primary-model genes showed markedly higher reselection probabilities than non-primary genes under both fixed-α and matched-sparsity conditions (Figure 1B,C). This result indicates that primary-model genes retain a strong relative selection advantage even when the precise composition of the sparse model varies across resampled cohorts. The persistence of this pattern after approximately controlling model sparsity further suggests that preferential reselection was not simply driven by changes in the number of selected genes as sample size decreased.

However, the stability results do not imply that the same 458 genes constitute an invariant signature that is recovered under every perturbation. Instead, they support the existence of a recurrent transcriptomic feature structure in which genes represented in the primary model are preferentially selected across resampled cohorts, while individual feature membership remains partly sample-dependent. Such behavior is compatible with sparse modeling of high-dimensional transcriptomic data, in which multiple correlated features can provide partially interchangeable representations of the same underlying biological variation. Consistently, when the regularization criterion itself was varied across models spanning training Spearman's ρ values of 0.7—0.9, primary-model genes remained strongly concentrated among the most consistently selected features (Fig. 1D), indicating that the observed feature preference was not dependent on the specific regularization setting used for the primary model.

Taken together, the weak transferability of absolute predicted BMI across cohorts, the modest out-of-sample performance even after prediction-oriented tuning, the preservation of an insulin-resistance-related signal in the independently projected transcriptomic space, and the preferential selection of primary-model genes across complementary resampling and regularization-sensitivity analyses suggest that the principal utility of the framework lies in identifying a reproducible BMI-anchored transcriptomic structure rather than in direct quantitative BMI prediction. Future iterations of the model would benefit from incorporating additional phenotypes such as insulin sensitivity, lipid profiles, or imaging-derived fat distribution. Moreover, our analysis focused primarily on adipose tissue transcriptomes, while obesity is a systemic condition involving multiple tissues and inter-organ communication [33—35]. Expanding to cross-tissue or single-cell data would further refine mechanistic insights.

On the other hand, the cross-species applicability in this study was an explicit design consideration in constructing the primary BMI-anchored transcriptomic model. We therefore restricted the model to transcriptomic features with high-confidence human—mouse orthology and did not include sex as an additional model predictor, because doing so would require carrying a non-transcriptomic covariate effect estimated in humans into the cross-species scoring framework. Nevertheless, because both human cohorts were predominant female, we directly evaluated whether omission of sex

 © 2026 The Authors. Published by Elsevier GmbH. This is an open access article under the CC BY-NC license (http://creativecommons.org/licenses/by-nc/4.0/).

materially influenced the observed transcriptomic structure. In the full primary cohort, explicit adjustment for sex produced minimal changes in gene selection and coefficient structure (Supplementary Information), while in the separate validation cohort the insulin-resistance-related PC1 difference was essentially unchanged after adjustment for sex (Supplementary Information). These sensitivity analyses suggest that female predominance is unlikely to account for the principal transcriptomic patterns observed here, although sex-specific biological effects cannot be excluded and should be examined further in larger, more sex-balanced cohorts. More broadly, although the cross-species validation provides an orthogonal assessment of the biological structure captured by the model, differences between human and mouse physiology still require cautious interpretation when translating these findings across species [15,36,37].

Looking forward, several avenues emerge. Functionally, the mitochondrial and protein translational pathways identified in MHO-like individuals represent attractive targets for therapeutic intervention or biomarker development. This is supported by transcriptomic studies identifying coordinated OXPHOS gene-set downregulation in human metabolic disease [38] and showing that short-term high-fat feeding suppresses mitochondrial/OXPHOS genes as an early molecular signature of diet-induced metabolic stress [39]. In parallel, translational control has emerged as a modifiable layer of adipose remodeling: PPARγ agonism can remodel translational machinery in adipose progenitors, but this response is impaired in obesity [40]. Methodologically, integrating transcriptomic predictors with other omics layers, such as epigenomics, proteomics, or metabolomics, could enhance predictive power and mechanistic resolution. Clinically, applying this framework to longitudinal cohorts may allow early identification of patients at risk for progression from metabolically healthy to unhealthy obesity, consistent with long-term prospective evidence that many initially metabolically healthy individuals transition to an unhealthy phenotype and that this conversion is accompanied by higher incident cardiovascular risk [41]. This view is reinforced by cohort analyses treating metabolic status as time-varying—highlighting the dynamic nature of "metabolic health" within obesity over extended follow-up [42]—and by detailed trajectory work describing transitions from healthy to unhealthy obesity and identifying clinical factors associated with conversion [43]. A systematic review/meta-analysis further synthesizes that MHO → MUO transition is common and that transitioners exhibit elevated CVD incidence, underscoring the value of early risk stratification and prevention windows [44].

In a broader perspective, this study underscores the utility of cross-species transcriptomics for disentangling the complex biology of obesity. By aligning human and mouse molecular states, we reveal conserved programs that distinguish protective from deleterious adiposity. Beyond obesity, this strategy may be generalized to other complex diseases where phenotypic heterogeneity complicates diagnosis and treatment. Ultimately, transcriptome-informed classification holds promise for moving obesity research and clinical care toward a more mechanistic and personalized paradigm.

In summary, we established a BMI-anchored transcriptomic framework that captures adiposity-linked molecular programs beyond gross anthropometric variation. Cross-species application showed that this framework reflects adiposity-specific transcriptional states rather than body size alone, distinguishing lipid-anabolic from oxidative-catabolic obesity phenotypes in mouse models. In humans, it resolved metabolically distinct obesity subgroups, linking MHO-like to mitochondrial and translational programs associated with resilience, and MUO-like to stress-adaptive, catabolic, and remodeling pathways associated with vulnerability. These findings support a conserved molecular axis underlying obesity heterogeneity and provide a basis for more biologically informed classification of metabolic disease.

4. METHODS

4.1. Human data

The human cohort consists of 1,479 omental visceral adipose tissue samples sourced from the Leipzig Obesity BioBank (LOBB; https://www.helmholtz-munich.de/en/hi-mag/cohort/leipzig-obesity-bio-bank-lobb), which were collected in a clinical setting within a cross-sectional framework. The cohort included 432 men (BMI 49.12 $\pm$ 9.1 kg/m^2; age 48.02 $\pm$ 11.8 years; 50.2% with T2D; 96.5% with BMI $\geq$30 kg/m^2) and 1,047 women (BMI 48.47 $\pm$ 8.8 kg/m^2; age 46.74 $\pm$ 11.8 years; 37.1% with T2D; 98.5% with BMI $\geq$30 kg/m^2). Participants underwent comprehensive clinical phenotyping with respect to obesity status, metabolic parameters, and anthropometric characteristics [32,45]. Adipose tissue samples were obtained during planned laparoscopic abdominal procedures, as previously reported [46]. Individuals were excluded if they were younger than 18 years, had a history of chronic drug or alcohol abuse, had smoked within the year prior to surgery, or presented with acute inflammatory conditions, advanced malignant disease, uncontrolled thyroid dysfunction, or Cushing's syndrome.

For evaluation in a separate, non-overlapping cohort, a set of LOBB participants with available hyperinsulinemic-euglycemic clamp data was analyzed as previously described [47]. None of these participants were included in the training cohort of primary modeling. The validation cohort comprised 77 individuals with obesity who were classified as insulin-sensitive (IS, n = 32; 71.8% female; age: 38.75 $\pm$ 10.98 years; BMI: 46.00 $\pm$ 6.82 kg/m^2; fasting plasma glucose (FPG): 5.22 $\pm$ 0.19 mmol/L; fasting plasma insulin (FPI): 28.74 $\pm$ 14.17 pmol/L) or insulin-resistant (IR, n = 45; 71.1% female; age: 47.09 $\pm$ 7.49 years; BMI: 46.89 $\pm$ 8.12 kg/m^2; FPG: 5.67 $\pm$ 0.34 mmol/L; FPI: 107.96 $\pm$ 30.32 pmol/L) according to glucose infusion rate (GIR) thresholds derived from the hyperinsulinemic-euglycemic clamp. RNA sequencing data generation and preprocessing were performed as described previously [47].

4.2. Library preparation and RNAseq analysis of human data

Total RNA was extracted from adipose tissue samples following the SMART-seq protocol (Switch Mechanisms at the 5' End of RNA Templates) [48]. Sequencing libraries were then constructed and subjected to single-end sequencing on a NovaSeq 6000 instrument at the Functional Genomics Centre Zurich.

Raw sequencing reads were processed with Fastp (v0.20.0) [49] to remove adapter sequences and low-quality bases. Quality trimming was performed as part of the same preprocessing workflow. The cleaned reads were then quantified with Kallisto (v0.46) [50,51]. Quantification was performed against the human reference genome GRCh38.p13. Gene model annotation was based on GENCODE release 32. Gene-level expression estimates obtained from Kallisto were used for downstream analyses.

Origin of mouse strains and housing conditions.

 © 2026 The Authors. Published by Elsevier GmbH. This is an open access article under the CC BY-NC license (http://creativecommons.org/licenses/by-nc/4.0/).

The mouse lines included in this study stem from a long-term selection experiment, which has been conducted in the Research Institute for Farm Animal Biology (FBN), generating, among others, mouse lines with increased body mass (DU6) [52] and protein mass (DU6P) [17]. These mice have been maintained for 180 generations in the case of DU6 (and 152 generations for DU6P) alongside an unselected control line (FZTDU) [17,53,54]. All animal procedures were performed in accordance with national and international guidelines and ethically approved by our own institutional board (Animal Protection Board from the Leibniz Institute for FBN). Mice were housed in a specific pathogen-free (SPF) environment with defined hygienic conditions at a temperature of 22.5 $\pm$ 0.2 °C, at least 40% humidity and a controlled light regime with a 12:12 h light—dark cycle. The mice were kept in polysulfone-cages of 365 $\times$ 207 $\times$ 140 mm (H-Temp PSU, Type II L, Eurostandard, Tecniplast, Germany) and had free access to pellet feed and water. Mice were fed ad libitum using a SBF (gross energy (GE) = 16.7 MJ kg^{-1}, metabolizable energy (ME) = 14.0 MJ kg^{-1}) including 12% fat, 27% protein, and 61% carbohydrates (ssniff® M-Z autoclavable, V1124-300, Soest, Germany) [17].

Male mice were sacrificed at 8—9 weeks of age, and inguinal and epigonadal white adipose tissue was resected and either immediately frozen for RNA isolation or fixed in 4% paraformaldehyde for histological analyses.

4.3. Data source and RNA sequencing of mouse lines

Tissue samples were collected from the DU mouse lines FZTDU, DU6, and DU6P, with six biological replicates per line. Library preparation was performed using the Illumina RNA preparation kit according to the manufacturer's protocol. Raw sequencing data were preprocessed using the nf-core/rnaseq pipeline. Read quality was evaluated using *FastQC*, and adapter sequences and low-quality bases were trimmed using *cutadapt*. Processed reads were aligned to the *Mus musculus* (GRCm39) reference genome using STAR, and quantification was performed using HTSeq.

4.4. Data preprocessing

To investigate pathways and functions related to human obesity mechanisms in mice, we developed a BMI-anchored transcriptomic model from human visceral adipose transcriptomes and subsequently applied it to mouse data. Protein-coding genes were extracted from the *Mus musculus* genome assembly (GRCm39) and the *Homo sapiens* genome assembly (GRCh38.p13). Genes with zero counts across all samples within a species were removed, yielding 19,884 human genes and 19,087 mouse genes for analysis.

Starting from the Kallisto-derived expression estimates, we applied quantile normalization separately to 1,479 human visceral adipose tissue samples and 18 mouse epigonadal adipose tissue samples (6 DU6, 6 DU6P, 6 FZTDU) to minimize expression-level perturbations and ensure comparable within-species distributions. Subsequently, feature-wise Z-score standardization was performed within each species to place all genes on a common scale, thereby reducing biases in cross-species transcriptomic model construction arising from intrinsic biological variation.

High-confidence orthologous gene pairs between human and mouse were retrieved from Ensembl Compara [55,56]. Orthologs were considered high confidence when supported by concordant gene-tree/species-tree reconciliation, sufficient sequence similarity and alignment coverage, conserved gene structure, and synteny across species. After orthology mapping, 16,042 high-confidence human—mouse orthologs were retained as features for subsequent BMI model development.

5. APPLICATION OF THE BMI-ANCHORED TRANSCRIPTOMIC MODEL TO MOUSE TRANSCRIPTOMES

To focus the analysis on obesity, we restricted the training set to individuals with BMI $\geq$30. Because extremely high BMI (morbid obesity) may reflect mechanistically distinct regimes of fat accumulation and metabolism, we further excluded the top 10% of BMI values to mitigate distributional shift and focus on the predominant cohort (Fig. S1). The resulting training set comprised 1,298 human visceral adipose samples with BMI 30—60.

Because the objective of this model was not clinical BMI prediction, but the construction of a BMI-anchored transcriptomic representation, model selection and interpretation emphasized rank preservation and biological interpretability rather than out-of-sample prediction accuracy. To obtain a sparse, transfer-ready signature, we fitted a LASSO (L1-regularized) linear regression model using BMI as the response variable and gene expression as predictors. Given the multifactorial nature of BMI and potential non-linearities at the global scale, model selection emphasized rank consistency, evaluating performance with Spearman's rank correlation (ρ). The regularization strength was tuned to achieve a Spearman's ρ of approximately 0.8 between predicted and measured BMI, thereby balancing parsimony and stability over marginal improvements in in-sample fit. The LASSO objective can be written as follows:

$$(\widehat{\beta_0}, \widehat{\beta}) = \arg\min_{\beta_0,\beta}\left[\frac{1}{2n}\sum_{i=1}^{n}\left(y_i - \beta_0 - \sum_{j=1}^{p} x_{ij}\beta_j\right)^2 + \alpha\sum_{j=1}^{p}|\beta_j|\right]$$

where x_{ij} denote the standardized expression of gene j in participant i, and y_i the measured BMI. Model coefficients were estimated by minimizing the LASSO objective. The regularization parameter α was selected to yield a Spearman correlation of approximately 0.8 between measured and model-predicted BMI, resulting in 458 genes with non-zero coefficients (Table S4). For participant i, predicted BMI was calculated as

$$\widehat{BMI_i} = \widehat{\beta_0} + \sum_{j\in S} x_{ij}\beta_j$$

where S denotes the set of 458 model-selected genes. All 1,298 participants in the primary modeling cohort were used to construct the final BMI-anchored transcriptomic model; no random training/test split was performed. This design reflected the objective of deriving a BMI-anchored transcriptomic representation rather than developing an out-of-sample clinical BMI predictor. The separate, non-overlapping validation cohort was not used for LASSO fitting or selection of the regularization parameter.

After training, we applied the learned human coefficients to the expression of the corresponding mouse orthologs, restricting to 458 genes with non-zero coefficients in the human model. For each mouse sample, the orthologous expression vector was aligned to the human feature set, and the linear predictor was used to project each mouse sample onto the human BMI-anchored transcriptomic axis, yielding a BMI-anchored transcriptomic score for each mouse sample. Line-level summaries were then examined across the three mouse lines (DU6, DU6P, FZTDU) for downstream analyses.

 © 2026 The Authors. Published by Elsevier GmbH. This is an open access article under the CC BY-NC license (http://creativecommons.org/licenses/by-nc/4.0/).

5.1. Identification of functional enrichment within model genes and group differences

To elucidate the biological processes represented by model-selected genes and group-specific differences, we performed gene set enrichment analysis (GSEA) [57]. This approach was used to identify biological functions enriched in association with the BMI-anchored model output as well as in group contrasts (e.g., DU6 vs. DU6P and MUO-like vs. MHO-like). Therefore, GSEA was applied to both model-selected genes and group-difference gene rankings, using Gene Ontology (GO) terms with a hierarchical depth greater than five to ensure adequate functional specificity. For model-based analyses, human genes selected by the model were ranked according to their regression coefficients. For group-difference analyses, genes were ranked using log2 fold changes.

For differential expression analysis, in the mouse dataset, where raw read counts were available, differential expression analysis was performed using DESeq2 [58], and genes were ranked by the resulting log2 fold changes. However, in the human dataset, where only Kallisto-derived expression values were available, group differences were quantified using expression-derived log2 fold-change–like effect sizes. Specifically, for each gene in each sample, expression was first scaled by the geometric mean of that gene within the corresponding group and then normalized by the within-sample median. Group-level effect sizes were subsequently calculated as the log2 ratio of the mean normalized expression values between groups. These human-derived effect sizes were used solely as the ranking metric for downstream GSEA and were not involved in model training.

For each analysis, an enrichment score (ES) was computed to quantify the degree to which a GO term was overrepresented within the ranked list. Statistical significance was assessed using 1,000 permutation tests, and ES values were standardized into z-scores as normalized enrichment score (NES). Functional modules with $z \geq 2$ were considered significantly enriched in the corresponding gene sets.

To determine whether the identified significantly enriched GO terms converged on biological processes relevant to obesity, we systematically mapped terms from the GSEA analysis to eleven predefined functional categories: (1) obesity/adiposity, (2) immune/inflammatory, (3) lipid metabolism/catabolism, (4) other metabolism, (5) energy production/consumption, (6) GH—IGF axis, (7) cell cycle/division, (8) cytoskeleton/adhesion, (9) development/signaling, (10) autophagy/protein quality control, and (11) miscellaneous. Terms were assigned to functional categories using a deterministic, rule-based text classification procedure based on the GO term description. For each term, the description was searched against a curated set of case-insensitive regular expression patterns. The classification was performed sequentially according to a fixed category priority order. If a term matched patterns from more than one category, the first matching category in the ordered rule set was assigned. The detailed mapping process is described in Supplementary.

5.2. Patient stratification using LOWESS-based discordance standardization

To address systematic bias between predicted BMI (BMI_p) and measured BMI (BMI_m), we employed locally weighted scatterplot smoothing (LOWESS) regression as a calibration approach. BMI_p values were treated as the independent variable (x), and BMI_m values as the dependent variable (y). A LOWESS curve was fitted using smoothing parameters of frac $= 0.3$ and it $= 0$. For each patient, we calculated the residual relative to the fitted curve:

$$r_i = BMI_m^i - f\left(BMI_p^i\right)$$

where BMI_m^i and BMI_p^i denote the measured and predicted BMI of participant i, respectively, and $f\left(BMI_p^i\right)$ represents the LOWESS-calibrated expected BMI conditional on BMI_p^i. Thus, r_i quantifies whether a patient's measured BMI is higher or lower than expected based on their predicted BMI. To account for heteroscedasticity, the conditional variance of residuals was estimated by applying LOWESS to the squared residuals, yielding local standard deviations $local_std\left(BMI_p^i\right)$. Each residual was standardized as:

$$z_i = \frac{r_i}{local_std\left(BMI_p^i\right)}$$

Because even standardized residuals may show systematic dependence on measured BMI, we performed an additional decile-based normalization. Participants were divided into deciles according to their measured BMI. Within each decile d, the mean μ_d and standard deviation σ_d of z_i were calculated, and each participant's standardized residual was further normalized:

$$z_{decile,i} = \frac{z_i - \mu_d}{\sigma_d}$$

This procedure allows patients to be evaluated relative to peers with similar BMI, thereby reducing systematic misclassification driven by regression to the mean. Final group assignments were based on the decile-standardized discordance score. Individuals with high positive scores were classified as transcriptome-defined MHO-like, indicating that their measured BMI was higher than expected from their BMI-anchored transcriptomic profile. Conversely, individuals with low negative scores were classified as transcriptome-defined MUO-like, indicating a more adverse transcriptomic state relative to their measured BMI. Individuals with scores between these thresholds were considered intermediate and were not assigned to either extreme phenotype:

$$-\text{MHO} - \text{like} : z_{decile,i} \geq 1$$

$$-\text{MUO} - \text{like} : z_{decile,i} \leq -1$$

$$-\text{intermediate} : -1 < z_{decile,i} < 1$$

This decile-standardization framework was used to stratify patients according to BMI-adjusted molecular-to-phenotypic discordance rather than residual patterns driven by regression to the mean.

For the separate validation cohort, the same LOWESS-based discordance procedure was applied independently using only the validation samples, including LOWESS fitting, residual calculation, and adjustment for heteroscedasticity. Because of the smaller sample size, the final normalization was performed within measured-BMI quartiles rather than deciles, yielding a quartile-standardized discordance score. The LOWESS fit and standardization parameters derived from the primary cohort were not applied to the validation cohort.

5.3. Projection of insulin-resistance–characterized samples into the primary-cohort PCA space

Principal component analysis was performed on the expression matrix of model-selected genes in the primary cohort. The resulting gene

 © 2026 The Authors. Published by Elsevier GmbH. This is an open access article under the CC BY-NC license (http://creativecommons.org/licenses/by-nc/4.0/).

loadings were retained as a fixed reference basis. Expression profiles from the insulin-resistance—characterized samples were processed using the corresponding model-selected genes and projected into this reference space by applying the PCA loadings derived exclusively from the primary cohort. No PCA model was refitted using the validation samples.

CRediT AUTHORSHIP CONTRIBUTION STATEMENT

Su Yin-Yuan: Writing — review & editing, Writing — original draft, Visualization, Methodology, Investigation, Formal analysis, Conceptualization. **Bundalian Linnaeus:** Writing — original draft, Visualization, Formal analysis. **Chen Yin-Cheng:** Writing — original draft, Visualization, Methodology, Investigation, Formal analysis. **Gjermeni Erind:** Writing — original draft. **Gille Benedikt:** Methodology. **Richter Sandy:** Data curation. **Jasaszwili Mariami:** Writing — review & editing, Visualization, Investigation, Data curation. **Palma-Vera Sergio Eliseo:** Resources, Data curation. **Hoffmann Anne:** Writing — review & editing, Formal analysis, Data curation. **Ghosh Adhideb:** Formal analysis, Data curation. **Wolfrum Christian:** Writing — review & editing, Resources. **Blüher Matthias:** Writing — review & editing, Resources, Funding acquisition. **Peleg Shahaf:** Writing — review & editing, Supervision, Resources, Project administration, Methodology. **Garten Antje:** Writing — review & editing, Visualization, Supervision, Project administration, Investigation, Funding acquisition, Conceptualization. **Le Duc Diana:** Writing — review & editing, Supervision, Project administration, Methodology, Funding acquisition, Conceptualization. **Lin Chen-Ching:** Writing — review & editing, Writing — original draft, Visualization, Supervision, Resources, Project administration, Methodology, Investigation, Funding acquisition, Formal analysis, Conceptualization.

AVAILABILITY OF DATA AND MATERIALS

Bulk RNAseq data from the LOBB reported in this study cannot be deposited in a public repository due to restrictions by patient consent. These restrictions are due to local data protection regulation in the written informed consent form tissue donors signed before taking part in the study. Access to human adipose tissue biobank data is regulated by the LOBB steering committee. Use of data is strictly limited to research purposes and not intended for commercialization. To request access, contact Matthias Blüher (matthias.blueher@medizin.uni-leipzig.de) or Anne Hoffmann (anne.hoffmann@helmholtz-munich.de).

ETHICS APPROVAL AND CONSENT TO PARTICIPATE

The LOBB study was approved by the Ethics Committee of the University of Leipzig (approval numbers: 159-12-21052012 and 017-12ek) and performed in accordance with the Declaration of Helsinki, the Bioethics Convention (Oviedo), and EU Directive on Clinical Trials (Directive 2001/20/EC). Written informed consent was obtained from all donors. All donors were informed of the purpose, risks and benefits of the biobank. Ethical guidelines and EU legislation for privacy and confidentiality in personal data collection and processing were followed, in particular directive 95/46/EC.

DECLARATION OF GENERATIVE AI AND AI-ASSISTED TECHNOLOGIES IN THE MANUSCRIPT PREPARATION PROCESS

During the preparation of this work, the authors used ChatGPT for English-language editing to improve the readability and clarity of the manuscript, as well as to assist in drafting and editing Python scripts to facilitate data analysis. No research data, tables, or figures were directly generated by ChatGPT. Following the use of this tool, the authors reviewed and edited the content as necessary and take full responsibility for the content of the published article.

DECLARATION OF COMPETING INTEREST

MB received personal honoraria from Amgen, AstraZeneca, Bayer, Boehringer Ingelheim, Lilly, Novo Nordisk, Novartis, and Sanofi as well as payments from Boehringer-Ingelheim to the institution. The remaining authors declare that the research was conducted in the absence of any commercial or financial relationships that could be construed as a potential conflict of interest.

APPENDIX A. SUPPLEMENTARY DATA

Supplementary data to this article can be found online at https://doi.org/10.1016/j.molmet.2026.102462.

DATA AVAILABILITY

Data will be made available on request.

REFERENCES

[1] Tahir UA, Gerszten RE. Molecular biomarkers for cardiometabolic disease: risk assessment in young individuals. Circ Res 2023;132(12):1663—73.

[2] World Health O. The top 10 causes of death. 2024.

[3] GBD 2019 Cancer Risk Factors Collaborators. The global burden of cancer attributable to risk factors, 2010-19: a systematic analysis for the Global Burden of Disease Study 2019. Lancet 2022;400(10352):563—91.

[4] Livingston G, Huntley J, Liu KY, Costafreda SG, Selbaek G, Alladi S, et al. Dementia prevention, intervention, and care: 2024 report of the Lancet standing Commission. Lancet 2024;404(10452):572—628.

[5] Ndumele CE, Rangaswami J, Chow SL, Neeland IJ, Tuttle KR, Khan SS, et al. Cardiovascular-Kidney-Metabolic health: a presidential advisory from the American heart Association. Circulation 2023;148(20):1606—35.

[6] Franks PW, Sargent JL. Diabetes and obesity: leveraging heterogeneity for precision medicine. Eur Heart J 2024;45(48):5146—55.

[7] Schulze MB, Stefan N. Metabolically healthy obesity: from epidemiology and mechanisms to clinical implications. Nat Rev Endocrinol 2024;20(11):633—46.

[8] World Health O. Obesity and overweight. 2024.

[9] Borgeson E, Tavajoh S, Lange S, Jessen N. The challenges of assessing adiposity in a clinical setting. Nat Rev Endocrinol 2024;20(10):615—26.

[10] Rubino F, Cummings DE, Eckel RH, Cohen RV, Wilding JPH, Brown WA, et al. Definition and diagnostic criteria of clinical obesity. Lancet Diabetes Endocrinol 2025;13(3):221—62.

[11] Lean ME, Leslie WS, Barnes AC, Brosnahan N, Thom G, McCombie L, et al. Primary care-led weight management for remission of type 2 diabetes (DiRECT): an open-label, cluster-randomised trial. Lancet 2018;391(10120):541—51.

[12] Taylor R, Holman RR. Normal weight individuals who develop type 2 diabetes: the personal fat threshold. Clin Sci (Lond) 2015;128(7):405—10.

[13] Taylor R, Barnes AC, Hollingsworth KG, Irvine KM, Solovyova AS, Clark L, et al. Aetiology of Type 2 diabetes in people with a 'normal' body mass index: testing the personal fat threshold hypothesis. Clin Sci (Lond) 2023;137(16):1333—46.

[14] Lean ME, Leslie WS, Barnes AC, Brosnahan N, Thom G, McCombie L, et al. 5-year follow-up of the randomised Diabetes Remission Clinical Trial (DiRECT)

 © 2026 The Authors. Published by Elsevier GmbH. This is an open access article under the CC BY-NC license (http://creativecommons.org/licenses/by-nc/4.0/).

of continued support for weight loss maintenance in the UK: an extension study. Lancet Diabetes Endocrinol 2024;12(4):233–46.
[15] Borgeson E, Boucher J, Hagberg CE. Of mice and men: pinpointing species differences in adipose tissue biology. Front Cell Dev Biol 2022;10:1003118.
[16] Loft A, Emont MP, Weinstock A, Divoux A, Ghosh A, Wagner A, et al. Towards a consensus atlas of human and mouse adipose tissue at single-cell resolution. Nat Metab 2025;7(5):875–94.
[17] Muller-Eigner A, Sanz-Moreno A, de-Diego I, Venkatasubramani AV, Langhammer M, Gerlini R, et al. Dietary intervention improves health metrics and life expectancy of the genetically obese Titan mouse. Commun Biol 2022;5(1):408.
[18] Gille B, Muller-Eigner A, Gottschalk S, Wytrwat E, Langhammer M, Peleg S. Titan mice as a model to test interventions that attenuate frailty and increase longevity. GeroScience 2024;46(4):3599–606.
[19] Gjermeni E, Fiebiger R, Bundalian L, Garten A, Schoneberg T, Le Duc D, et al. The impact of dietary interventions on cardiometabolic health. Cardiovasc Diabetol 2025;24(1):234.
[20] Sawitzky M, Zeissler A, Langhammer M, Bielohuby M, Stock P, Hammon HM, et al. Phenotype selection reveals coevolution of muscle glycogen and protein and PTEN as a gate keeper for the accretion of muscle mass in adult female mice. PLoS One 2012;7(6):e39711.
[21] Khawaja T, Nied M, Wilgor A, Neeland IJ. Impact of visceral and hepatic fat on cardiometabolic health. Curr Cardiol Rep 2024;26(11):1297–307.
[22] Kubota S, Yabe D. Visceral adipose tissue quality and its impact on Metabolic health. J Clin Endocrinol Metab 2024;109(8):e1665–6.
[23] Lee MJ, Kim J. The pathophysiology of visceral adipose tissues in cardiometabolic diseases. Biochem Pharmacol 2024;222:116116.
[24] Das SK, Ma L, Sharma NK. Adipose tissue gene expression and metabolic health of obese adults. Int J Obes 2015;39(5):869–73.
[25] Zhou Q, Fu Z, Gong Y, Seshachalam VP, Li J, Ma Y, et al. Metabolic health status contributes to transcriptome alternation in human visceral adipose tissue during obesity. Obesity 2020;28(11):2153–62.
[26] Rosendo-Silva D, Gomes PB, Rodrigues T, Viana S, da Costa AN, Scherer PE, et al. Clinical and molecular profiling of human visceral adipose tissue reveals impairment of vascular architecture and remodeling as an early hallmark of dysfunction. Metabolism 2024;153:155788.
[27] Meroni M, Chiappori F, Paolini E, Longo M, De Caro E, Mosca E, et al. A novel gene signature to diagnose MASLD in metabolically unhealthy obese individuals. Biochem Pharmacol 2023;218:115925.
[28] Acharjee A, Wijesinghe SN, Russ D, Gkoutos G, Jones SW. Cross-species transcriptomics identifies obesity associated genes between human and mouse studies. J Transl Med 2024;22(1):592.
[29] Liu H, Xing K, Jiang Y, Liu Y, Wang C, Ding X. Using machine learning to identify biomarkers affecting fat deposition in pigs by integrating Multisource transcriptome information. J Agric Food Chem 2022;70(33):10359–70.
[30] Wang Y, Zhang J, Yang X, Wang F, Jin L, Li J, et al. Obesity induced transcriptional changes in skeletal muscle across different species. PLoS One 2025;20(7):e0327988.
[31] Romero-Corral A, Somers VK, Sierra-Johnson J, Thomas RJ, Collazo-Clavell ML, Korinek J, et al. Accuracy of body mass index in diagnosing obesity in the adult general population. Int J Obes 2008;32(6):959–66.
[32] Bluher M. Metabolically healthy obesity. Endocr Rev 2020;41(3).
[33] Jia Z, Wang Z, Pan H, Zhang J, Wang Q, Zhou C, et al. Crosstalk between fat tissue and muscle, brain, liver, and heart in obesity: cellular and molecular perspectives. Eur J Med Res 2024;29(1):637.
[34] Priest C, Tontonoz P. Inter-organ cross-talk in metabolic syndrome. Nat Metab 2019;1(12):1177–88.
[35] Wang S, Liu Y, Chen J, He Y, Ma W, Liu X, et al. Effects of multi-organ crosstalk on the physiology and pathology of adipose tissue. Front Endocrinol 2023;14:1198984.
[36] Lempesis IG, Tsilingiris D, Liu J, Dalamaga M. Of mice and men: considerations on adipose tissue physiology in animal models of obesity and human studies. Metabol Open 2022;15:100208.
[37] Delhanty PJD, Visser JA. Navigating the strengths and constraints of mouse models in obesity research. Endocrinology 2025;166(9).
[38] Mootha VK, Lindgren CM, Eriksson KF, Subramanian A, Sihag S, Lehar J, et al. PGC-1alpha-responsive genes involved in oxidative phosphorylation are coordinately downregulated in human diabetes. Nat Genet 2003;34(3):267–73.
[39] Sparks LM, Xie H, Koza RA, Mynatt R, Hulver MW, Bray GA, et al. A high-fat diet coordinately downregulates genes required for mitochondrial oxidative phosphorylation in skeletal muscle. Diabetes 2005;54(7):1926–33.
[40] De Siqueira MK, Li G, Zhao Y, Wang S, Ahn IS, Tamboline M, et al. PPAR-gamma-dependent remodeling of translational machinery in adipose progenitors is impaired in obesity. Cell Rep 2024;43(12):114945.
[41] Eckel N, Li Y, Kuxhaus O, Stefan N, Hu FB, Schulze MB. Transition from metabolic healthy to unhealthy phenotypes and association with cardiovascular disease risk across BMI categories in 90 257 women (the Nurses' Health Study): 30 year follow-up from a prospective cohort study. Lancet Diabetes Endocrinol 2018;6(9):714–24.
[42] Hinnouho GM, Czernichow S, Dugravot A, Nabi H, Brunner EJ, Kivimaki M, et al. Metabolically healthy obesity and the risk of cardiovascular disease and type 2 diabetes: the Whitehall II cohort study. Eur Heart J 2015;36(9):551–9.
[43] Mendes FD, Dos Santos HC, Mill JG, Molina M, Diniz M, Quintino CR, et al. From healthy to unhealthy obesity: a longitudinal study of adults in ELSA-Brasil. PLOS Glob Publ Health 2025;5(4):e0004325.
[44] Abiri B, Koohi F, Ebadinejad A, Valizadeh M, Hosseinpanah F. Transition from metabolically healthy to unhealthy overweight/obesity and risk of cardiovascular disease incidence: a systematic review and meta-analysis. Nutr Metabol Cardiovasc Dis 2022;32(9):2041–51.
[45] Kloting N, Fasshauer M, Dietrich A, Kovacs P, Schon MR, Kern M, et al. Insulin-sensitive obesity. Am J Physiol Endocrinol Metab 2010;299(3):E506–15.
[46] Langhardt J, Flehmig G, Kloting N, Lehmann S, Ebert T, Kern M, et al. Effects of weight loss on glutathione peroxidase 3 serum concentrations and adipose tissue expression in human obesity. Obes Facts 2018;11(6):475–90.
[47] Reinisch I, Ghosh A, Noe F, Sun W, Dong H, Leary P, et al. Unveiling adipose populations linked to metabolic health in obesity. Cell Metab 2025;37(3):640–655 e644.
[48] Picelli S, Faridani OR, Bjorklund AK, Winberg G, Sagasser S, Sandberg R. Full-length RNA-seq from single cells using Smart-seq2. Nat Protoc 2014;9(1):171–81.
[49] Chen S, Zhou Y, Chen Y, Gu J. Fastp: an ultra-fast all-in-one FASTQ preprocessor. Bioinformatics 2018;34(17):i884–90.
[50] Rajcsanyi LS, Hoffmann A, Ghosh A, Matrisch-Dinkler B, Zheng Y, Peters T, et al. Genetic variants in genes involved in creatine biosynthesis in patients with severe obesity or anorexia nervosa. Front Genet 2023;14:1128133.
[51] Bray NL, Pimentel H, Melsted P, Pachter L. Near-optimal probabilistic RNA-seq quantification. Nat Biotechnol 2016;34(5):525–7.
[52] Renne U, Langhammer M, Brenmoehl J, Walz C, Zeissler A, Tuchscherer A, et al. Lifelong obesity in a polygenic mouse model prevents age- and diet-induced glucose intolerance- obesity is no road to late-onset diabetes in mice. PLoS One 2013;8(11):e79788.
[53] Schueler L. Mouse strain Fzt:DU and its use as model in animal breeding research. Archiv Tierzucht 1985;28:357–63.
[54] Dietl G, Langhammer M, Renne U. Model simulations for genetic random drift in the outbred strain Fzt: DU. Archiv Tierzucht 2004;47(6):595–604.
[55] Vilella AJ, Severin J, Ureta-Vidal A, Heng L, Durbin R, Birney E. EnsemblCompara GeneTrees: complete, duplication-aware phylogenetic trees in vertebrates. Genome Res 2009;19(2):327–35.

 © 2026 The Authors. Published by Elsevier GmbH. This is an open access article under the CC BY-NC license (http://creativecommons.org/licenses/by-nc/4.0/).

[56] Harrison PW, Amode MR, Austine-Orimoloye O, Azov AG, Barba M, Barnes I, et al. Ensembl 2024. Nucleic Acids Res 2024;52(D1):D891–9.
[57] Subramanian A, Tamayo P, Mootha VK, Mukherjee S, Ebert BL, Gillette MA, et al. Gene set enrichment analysis: a knowledge-based approach for interpreting genome-wide expression profiles. Proc Natl Acad Sci U S A 2005;102(43):15545–50.
[58] Love MI, Huber W, Anders S. Moderated estimation of fold change and dispersion for RNA-seq data with DESeq2. Genome Biol 2014;15(12):550.

 © 2026 The Authors. Published by Elsevier GmbH. This is an open access article under the CC BY-NC license (http://creativecommons.org/licenses/by-nc/4.0/).